mathematics

MDPI

Article

Three-Dimensional Hydro-Magnetic Flow Arising in a Long Porous Slider and a Circular Porous Slider with Velocity Slip

Naeem Faraz [1,*], Yasir Khan [2], Amna Anjum [1,3,*] and Muhammad Kahshan [4,5]

1 International Cultural Exchange School (ICES), Donghua University, West Yan'an Road 1882, Shanghai 200051, China
2 Department of Mathematics, University of Hafr Al-Batin, Hafr Al-Batin 31991, Saudi Arabia
3 Glorious Sun School of Business and Management, Donghua University, West Yan'an Road 1882, Shanghai 200051, China
4 Faculty of Science, Jiangsu University, Zhenjiang 212013, China
5 Department of Mathematics, COMSATS University Islamabad, Abbottabad 22060, Pakistan
* Correspondence: nfaraz_math@yahoo.com or naeem@dhu.edu.cn (N.F.); amnaeem14@gmail.com (A.A.); Tel.: +86-150-0075-1065 (N.F.); +86-132-6289-1913 (A.A.)

Received: 21 July 2019; Accepted: 12 August 2019; Published: 16 August 2019

Abstract: The current research explores the injection of a viscous fluid through a moving flat plate with a transverse uniform magneto-hydrodynamic (MHD) flow field to reduce sliding drag. Two cases of velocity slip between the slider and the ground are studied: a long slider and a circular slider. Solving the porous slider problem is applicable to fluid-cushioned porous sliders, which are useful in reducing the frictional resistance of moving bodies. By using a similarity transformation, three dimensional Navier–Stokes equations are converted into coupled nonlinear ordinary differential equations. The resulting nonlinear boundary value problem was solved analytically using the homotopy analysis method (HAM). The HAM provided a fast convergent series solution, showing that this method is efficient, accurate, and has many advantages over the other existing methods. Solutions were obtained for the different values of Reynolds numbers (R), velocity slip, and magnetic fields. It was found that surface slip and Reynolds number had substantial influence on the lift and drag of the long and the circular sliders. Moreover, the effects of the applied magnetic field on the velocity components, load-carrying capacity, and friction force are discussed in detail with the aid of graphs and tables.

Keywords: porous slider; MHD flow; reynolds number; velocity slip; homotopy analysis method

1. Introduction

It is a well-established fact that a moving body reduces drag if it is elevated by a layer of air. This phenomenon is used in air-cushioned vehicles and in air hockey, in which the frictional resistance of moving objects is reduced. Skalak and Wang [1] were the pioneers of studying the three-dimensional flow that arises between a moving porous flat plate and the ground, and they later on wrote an erratum on their own paper [2]. Wang also studied elliptical porous sliders [3]. In the case of Newtonian fluids, past studies have included porous circular, long, inclined, and elliptical sliders. R. C. Bhattacharjee studied a porous slider bearing lubricated with a coupled stress (a magneto-hydrodynamic (MHD) fluid) [4]. Jimit made a comparison of the different porous structures on the performance of a magnetic fluid [5]. Prawal Sinha analyzed the thermal effects of a long porous rough slider bearing [6]. Mohmmadrayian analyzed a rough porous inclined slider bearing lubricated with a ferrofluid in consideration of slip velocity [7]. Ji Lang both theoretically and experimentally

investigated the transient squeezing flow in a highly porous film [8]. Similarly, a large amount of literature is available in relation to long porous sliders (LPSs) [1,6,9–13] and circular porous sliders (CPSs) [2,14–18]. Awati investigated the lubrication of a long porous slider by using the homotopy analysis method (HAM) [10]. In a separate study, Khan studied the effects of Reynolds numbers by using different analytical methods [11,12]. Naeem studied the influence of Reynolds numbers (R) on long [13] and circular porous sliders [18]. Ghoreishi studied the circular slider [14]. Madani investigated the circular porous slider by using HPM, and also analyzed its lift and drag [19].

All the above mentioned studies were done without a slip condition on either the immobile ground or slider. However, a slip condition is essential for super-hydrophobic planes, as it is difficult to have a zero mean tangential velocity from where the fluid is injected when there is a slip. Furthermore, in order to minimize adhesion, the fluid could be a rarefied gas, where the compact exterior could be coated with a material, or the ground could be uneven so that an equivalent slip exists or there is a slip flow regime. Wang [16] discussed slip effects, but didn't consider the effects of a transverse magnetic field. Therefore, the goal of the current work is to examine the impact of slip and Reynolds numbers when a transverse magnetic field is affecting the performance of a porous slider. Through the literature survey, it is assumed that a three-dimensional flow with slip and a uniform magnetic field does not exist. Hence, the goal of the current research is to analyze the performance of porous sliders in the presence of slip and a Reynolds number with a constant magnetic field, and to assess their effects on the components of velocity lift and drag.

The structure of the article is as follows: In the introduction, a brief history of the problem of the porous slider and its application is presented. In the second section, the formulation of the problems are given, while in the third section the formulation of a homotopic solution is presented [20]. The fourth section deals with the convergence criteria of the HAM. Results and discussions are given in the fifth section. Finally, the conclusion is given in the sixth section, with a list of nomenclature.

As discussed above, the velocity slip condition is considered in this study. Navier introduced the slip condition for the first time as follows:

$$x_1 = H\varsigma \tag{1}$$

In Equation (1), tangential velocity u is proportional to the shear stress and H is the constant of proportionality, which is actually a slip coefficient. In order to ignore the end effects, it is assumed that the gap between slider and ground is quite small as compared to the slider's lateral dimension. Both circular and long porous sliders are considered in this study.

2. Problem Formulation of Long and Circular Sliders

In this study, the incompressible and steady flow of a viscous fluid between porous (long and circular) sliders and the ground is considered in the presence of a uniform magnetic field, as shown in Figure 1.

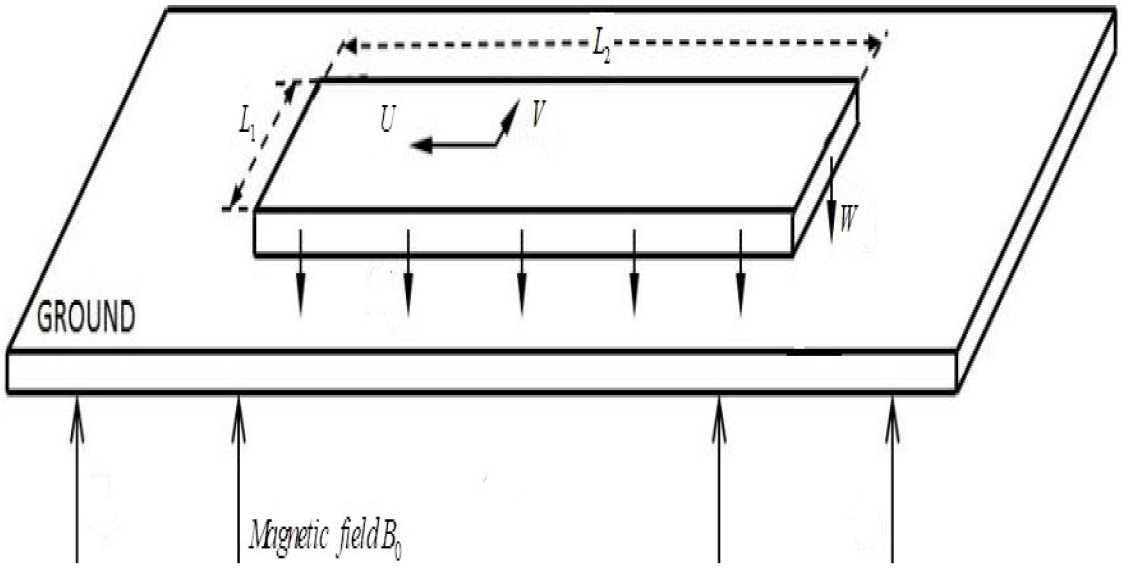

(**a**)

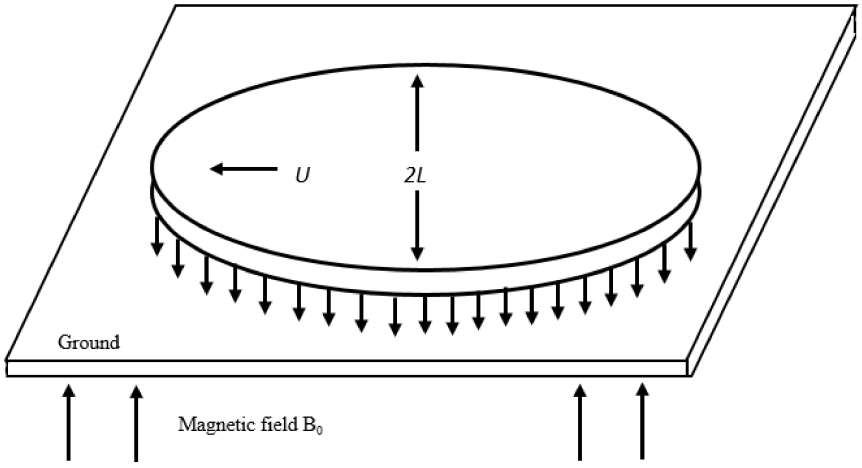

(**b**)

Figure 1. (**a**) Schematic diagram of the movement of a long porous slider (LPS). (**b**) Schematic diagram of the movement of a circular porous slider (CPS).

Length and width are quite big compared to height d. The slider moves with the velocity components and is elevated because of the injection of fluid from below with a magnetic field applied externally. In order to avoid the induced magnetic field formed by the movement of the fluid, it is assumed that the magnetic Reynolds number is not very big. Furthermore, the induced and imposed electric field are supposed to be negligible, and therefore the electromagnetic body force per unit volume simplifies $\mathrm{F}_{em} = \sigma_0(\mathrm{v} \times \mathrm{B}) \times \mathrm{B}$, where $\mathrm{B} = (0, 0, B_0)$ is the magnetic field.

Under the above-stated assumptions and conditions, Navier–Stokes equations take the following form:

$$\phi_1 \frac{\partial \phi_1}{\partial x_1} + \phi_2 \frac{\partial \phi_1}{\partial x_2} + \phi_3 \frac{\partial \phi_1}{\partial x_3} = -\frac{1}{\rho} \frac{\partial p}{\partial x_1} + \upsilon \left(\frac{\partial^2 \phi_1}{\partial x_1^2} + \frac{\partial^2 \phi_1}{\partial x_2^2} + \frac{\partial^2 \phi_1}{\partial x_3^2} \right) - \frac{\sigma_0}{\rho} B_0^2 \phi_1 \tag{2}$$

$$\phi_1 \frac{\partial \phi_2}{\partial x_1} + \phi_2 \frac{\partial \phi_2}{\partial x_2} + \phi_3 \frac{\partial \phi_2}{\partial x_3} = -\frac{1}{\rho} \frac{\partial p}{\partial x_2} + \upsilon \left(\frac{\partial^2 \phi_2}{\partial x_1^2} + \frac{\partial^2 \phi_2}{\partial x_2^2} + \frac{\partial^2 \phi_2}{\partial x_3^2} \right) - \frac{\sigma_0}{\rho} B_0^2 \phi_2 \tag{3}$$

$$\phi_1\frac{\partial\phi_3}{\partial x_1}+\phi_2\frac{\partial\phi_3}{\partial x_2}+\phi_3\frac{\partial\phi_3}{\partial x_3}=-\frac{1}{\rho}\frac{\partial p}{\partial x_3}+\upsilon\left(\frac{\partial^2\phi_3}{\partial x_1^2}+\frac{\partial^2\phi_3}{\partial x_2^2}+\frac{\partial^2\phi_3}{\partial x_3^2}\right) \tag{4}$$

Velocity components are expressed as (ϕ_1,ϕ_2,ϕ_3), where ρ, p, and υ are density, pressure and kinematic viscosity, respectively. Law of conservation of mass is as follows:

$$\frac{\partial\phi_1}{\partial x_1}+\frac{\partial\phi_2}{\partial x_2}+\frac{\partial\phi_3}{\partial x_3}=0 \tag{5}$$

According to Naeem [13], the following transform has been used:

$$\phi_1=U\psi_1(\varsigma)+\frac{W}{d}x_1{\psi_3}'(\varsigma),\phi_2=V\psi_2(\varsigma),\phi_3=-W\psi_3(\varsigma). \tag{6}$$

where $\varsigma=\frac{x_3}{d}$. By adding Equation (6) into Equations (2)–(4), the following ordinary differential equations are obtained:

$$\psi_3^{iv}=R\left(\psi_3'\psi_3''-\psi_3\psi_3'''\right)+M^2\psi_3' \tag{7}$$

$$\psi_1''=R\left(\psi_1\psi_3'-\psi_3\psi_1'\right)+M^2\psi_1 \tag{8}$$

$$\psi_2''=-R\left(\psi_1\psi_2'\right)+M^2\psi_2 \tag{9}$$

where R is the Reynolds number ($R=Wd/\upsilon$). Boundary conditions at $x_3=0$ and $x_3=d$ are given in Equations (10) and (11), respectively.

$$\phi_1=U+H_1\mu\frac{\partial\phi_1}{\partial x_3},\quad \phi_2=V+H_1\mu\frac{\partial\phi_2}{\partial x_3},\quad \phi_3=0 \tag{10}$$

$$\phi_1=-H_2\mu\frac{\partial\phi_1}{\partial x_3},\quad \phi_2=-H_2\mu\frac{\partial\phi_2}{\partial x_3}=0,\quad \phi_3=-W \tag{11}$$

where H_1, H_2, and $\mu=\rho\upsilon$ are slip coefficients and viscosity, respectively. Equations (10) and (11) take the following form:

$$\begin{array}{l}\psi_3'(0)=\beta_1\psi_3''(0)=,\psi_3(0)=0,\\ \psi_3(1)=1,\psi_3'(1)=-\beta_2\psi_3''(1),\\ \psi_1(1)=-\beta_2\psi_1'(1),\psi_1(0)-1=\beta_1\psi_1'(0),\\ \psi_2(1)=-\beta_2\psi_2'(1),\psi_2(0)-1=\beta_1\psi_2'(0).\end{array} \tag{12}$$

where $\beta_1=H_1\mu/d,\beta_2=H_2\mu/d$ are slip factors. Equations (7)–(9) and (12) will be solved by the HAM. The expression for pressure can be deduced from Equations (2)–(4) as follows:

$$-\frac{p}{\rho}=\frac{W^2\Lambda x_1^2}{2d}+\frac{1}{2}\phi_3^2-\gamma\phi_{3,x_3}+A \tag{13}$$

where Λ,A are constants and

$$\Lambda=\left(\psi_3'\right)^2-\psi_3\psi_3''-\frac{1}{R}\psi_3'''=\left(\psi_3'(0)\right)^2-\frac{1}{R}\psi_3'''(0). \tag{14}$$

If $2l$ is the width of the slider with ambient pressure ρ_0, then Equation (13) gives

$$p-p_0=-\rho\frac{\Lambda W^2\left(x_1^2-l^2\right)}{2d^2}. \tag{15}$$

The relationship between depth and lift can be expressed as follows:

$$L = \int_{-1}^{1} (p - p_0) dx = \frac{2\rho W^2 l^3}{3d^2} \Lambda. \tag{16}$$

where $2\rho W^2 l^3 / \left(3d^2\right)$ is normalized factor. The relationship between depth and drag in the x_1- direction is

$$D_{x_1} = -\int_{-1}^{1} \mu \frac{\partial \phi_1}{\partial x_3} |_{z=d} dx_1 = -\frac{2\mu U l}{d} \psi_1^{/}(1). \tag{17}$$

Similarly, $2\mu Ul/d$ is the normalized factor of drag in the x_1- direction, which is $-\psi_1^{/}(1)$, while $-\psi_2^{/}(1)$ is normalized drag for the x_2- direction:

$$D_{x_2} = -\int_{-1}^{1} \mu \frac{\partial \phi_2}{\partial x_3} |_{z=d} dx_1 = -\frac{2\mu V l}{d} \psi_2^{/}(1). \tag{18}$$

Similarly, from Figure 1b, a circular slider can be seen, where L is the radius of the slider (which can be assumed to be comparatively bigger than the width). Since the slider is levitated, the axes on the slider can be fixed so that the ground is moving with a velocity component in the x_1- direction. For the circular slider, a similar transform [18] helps to reduce the partial differential equations into ordinary differential equations:

$$x_1 = U\psi_5(\varsigma) + \frac{W}{d} x_1 \psi_4^{/}(\varsigma), x_2 = \frac{W}{d} x_2 \psi_4^{/}(\varsigma), x_3 = -2W\psi_4(\varsigma). \tag{19}$$

With the help of Equation (19), Equations (2)–(4) take the following form

$$\psi_4^{iv} - 2R\psi_4 \psi_4^{///} - M^2 \psi_4^{/} = 0 \tag{20}$$

$$\psi_5^{//} - R\left(\psi_5 \psi_4^{/} - 2\psi_4 \psi_5^{/}\right) - M^2 \psi_5 = 0 \tag{21}$$

$$-\frac{p}{\rho} = \frac{W^2 \Lambda (x_1^2 + x_2^2)}{2d} + \frac{1}{2} x_3^2 - \gamma x_{3,x_3} + C \tag{22}$$

in which Λ, C are constants and

$$\Lambda_1 = \left(\psi_4^{/}(0)\right)^2 - \frac{1}{R} \psi_4^{///}(0). \tag{23}$$

The boundary conditions on $x_3 = 0 \& d$:

$$\begin{array}{l} \psi_4^{/}(0) = \beta_1 \psi_4^{//}(0) =, \psi_4(0) = 0, \\ \psi_4(1) = 1/2, \psi_4^{/}(1) = -\beta_2 \psi_4^{//}(1), \\ \psi_5(1) = -\beta_2 \psi_5^{/}(1), \psi_5(0) - 1 = \beta_1 \psi_5^{/}(0). \end{array} \tag{24}$$

To normalize the lift, integrating the bottom of the slider as a result of the normalized factor can be expressed as $\pi\rho W^2 l^4 / 4d$.

$$L = \frac{4d}{\pi \rho W^2 l^4} \iint_s (p - p_0) ds = \frac{1}{R^3} \Lambda. \tag{25}$$

The relationship between depth and drag in the x_1- direction is

$$D_{x_1} = \frac{d}{\pi \mu U l^2} \iint_s H_{x_3 x_1} ds = -\frac{1}{R^3} \psi_5^{/}(1). \tag{26}$$

3. Homotopic Solution Procedure

To apply HAM [20], the following initial guesses for Equations (7)–(9), (20), and (21) can be chosen as

$$\begin{array}{l}\psi_{3,0}(\varsigma)=\frac{-2\varsigma^3(1+\beta_1+\beta_2)+3\varsigma(1+2\beta_2)(\varsigma+2\beta_1)}{1+4(\beta_1+\beta_2)+12\beta_1\beta_2},\\ \psi_{1,0}(\varsigma)=\frac{1-\varsigma+\beta_2}{1+\beta_1+\beta_2},\psi_{2,0}(\varsigma)=\frac{1-\varsigma+\beta_2}{1+\beta_1+\beta_2},\\ \psi_{4,0}(\varsigma)=\frac{-2\varsigma^3(1+\beta_1+\beta_2)+3\varsigma(1+2\beta_2)(\varsigma+2\beta_1)}{2(1+4(\beta_1+\beta_2)+12\beta_1\beta_2)},\psi_{5,0}(\varsigma)=\frac{1-\varsigma+\beta_2}{1+\beta_1+\beta_2}\end{array} \tag{27}$$

For the initial approximation, the following auxiliary linear operators can be chosen:

$$\begin{array}{l}L(\psi_3)=\frac{d^4h}{d\varsigma^4},L(\psi_1)=\frac{d^2\theta}{d\varsigma^2},L(\psi_2)=\frac{d^2\theta}{d\varsigma^2},\\ L(\psi_4)=\frac{d^4\theta}{d\varsigma^4},L(\psi_5)=\frac{d^2\theta}{d\varsigma^2}.\end{array} \tag{28}$$

which satisfies

$$\begin{array}{l}L_{\psi_1}[A_5+A_6\varsigma]=0,L_{\psi_2}[A_7+A_8\varsigma]=0,\\ L_{\psi_3}\Big[A_1+A_2\varsigma+A_3\varsigma^2+A_4\varsigma^4\Big]=0,\\ L_{\psi_4}\Big[A_9+A_{10}\varsigma+A_{11}\varsigma^2+A_{12}\varsigma^4\Big]=0,L_{\psi_5}[A_{13}+A_{14}\varsigma]=0.\end{array} \tag{29}$$

in which $A_i(i=1-14)$ are constants of integration.

Initial Order Deformation Problem

The deformation equations for the initial order can be viewed as follows:

$$(1-\Phi)L_{\psi_1}\Big[\widehat{\psi}_1(\varsigma,\Phi)-\widehat{\psi}_{1,0}(\varsigma,\Phi)\Big]=\Phi\hbar_{\psi_1}H_{\psi_1}N_{\psi_1}\Big[\widehat{\psi}_1(\varsigma,\Phi)\Big] \tag{30}$$

$$(1-\Phi)L_{\psi_2}\Big[\widehat{\psi}_2(\varsigma,\Phi)-\widehat{\psi}_{2,0}(\varsigma,\Phi)\Big]=\Phi\hbar_{\psi_2}H_{\psi_2}N_{\psi_2}\Big[\widehat{\psi}_2(\varsigma,\Phi)\Big] \tag{31}$$

$$(1-\Phi)L_{\psi_3}\Big[\widehat{\psi}_3(\varsigma,\Phi)-\widehat{\psi}_{3,0}(\varsigma,\Phi)\Big]=\Phi\hbar_{\psi_3}H_{\psi_3}N_{\psi_3}\Big[\widehat{\psi}_3(\varsigma,\Phi)\Big] \tag{32}$$

$$(1-\Phi)L_{\psi_4}\Big[\widehat{\psi}_4(\varsigma,\Phi)-\widehat{\psi}_{4,0}(\varsigma,\Phi)\Big]=\Phi\hbar_{\psi_4}H_{\psi_4}N_{\psi_4}\Big[\widehat{\psi}_4(\varsigma,\Phi)\Big] \tag{33}$$

$$(1-\Phi)L_{\psi_5}\Big[\widehat{\psi}_5(\varsigma,\Phi)-\widehat{\psi}_{5,0}(\varsigma,\Phi)\Big]=\Phi\hbar_{\psi_5}H_{\psi_5}N_{\psi_5}\Big[\widehat{\psi}_5(\varsigma,\Phi)\Big] \tag{34}$$

and the boundary conditions are

$$\widehat{\psi}_1(1,\Phi)=-\mu_2\widehat{\psi}_1^{/}(1,\Phi),\ \widehat{\psi}_1(0,\Phi)-1=-\mu_1\widehat{\psi}_1^{/}(0,\Phi) \tag{35}$$

$$\widehat{\psi}_2^{/}(0,\Phi)-1=-\mu_1\widehat{\psi}_2^{/}(0,\Phi),\ \widehat{\psi}_2(1,\Phi)=-\mu_2\widehat{\psi}_2^{/}(1,\Phi) \tag{36}$$

$$\widehat{\psi}_3^{/}(0,\Phi)=\mu_1\widehat{\psi}_3^{//}(0,\Phi),\widehat{\psi}_3(0,\Phi)=0,\widehat{\psi}_3(1,\Phi)=1,\widehat{\psi}_3^{/}(1,\Phi)=-\mu_2\widehat{\psi}_3^{//}(1,\Phi) \tag{37}$$

$$\widehat{\psi}_4^{/}(0,\Phi)=\mu_1\widehat{\psi}_4^{//}(0,\Phi),\widehat{\psi}_4(0,\Phi)=0,\widehat{\psi}_4(1,\Phi)=1/2,\widehat{\psi}_4^{/}(1,\Phi)=-\mu_2\widehat{\psi}_4^{//}(1,\Phi), \tag{38}$$

$$\widehat{\psi}_5(1,\Phi)=-\mu_2\widehat{\psi}_5^{/}(1,\Phi),\widehat{\psi}_5(0,\Phi)-1=-\mu_1\widehat{\psi}_5^{/}(0,\Phi) \tag{39}$$

where $N_{\psi_1},N_{\psi_2},N_{\psi_3},N_{\psi_4}$, and N_{ψ_5} are defined as

$$N_{\psi_3}\Big[\widehat{\psi}_3(\varsigma;\Phi)\Big]=\widehat{\psi}_3{}^{////}-R\Big(\widehat{\psi}_3{}^{/}\widehat{\psi}_3{}^{//}-\widehat{\psi}_3\widehat{\psi}_3{}^{///}\Big)-M^2\psi_3^{/} \tag{40}$$

$$N_{\widehat{\psi}_1}\Big[\widehat{\psi}_1(\varsigma;\Phi)\Big]=\widehat{\psi}_1{}^{//}-R\Big(\widehat{\psi}_1\widehat{\psi}_3{}^{/}-\widehat{\psi}_3\widehat{\psi}_1{}^{/}\Big)-M^2\psi_1, \tag{41}$$

$$N_{\widehat{\psi}_2}\Big[\widehat{\psi}_2(\varsigma;\Phi)\Big] = \widehat{\psi}_2{}'' + R\Big(\widehat{\psi}_3\widehat{\psi}_2{}'\Big) - M^2\psi_2, \tag{42}$$

$$N_{\psi_4}\Big[\widehat{\psi}_4(\varsigma;\Phi)\Big] = \widehat{\psi}_4{}'''' - 2R\widehat{\psi}_4\widehat{\psi}_4{}''' - M^2\widehat{\psi}_4{}' \tag{43}$$

$$N_{\psi_5}\Big[\widehat{\psi}_5(\varsigma;\Phi)\Big] = \widehat{\psi}_5{}'' - R\Big(\widehat{\psi}_5\widehat{\psi}_4{}' - 2\widehat{\psi}_4\widehat{\psi}_5{}'\Big) - M^2\widehat{\psi}_5 \tag{44}$$

Here, the auxiliary parameters are $\hbar_{\psi_1} \neq 0, \hbar_{\psi_2} \neq 0, \hbar_{\psi_3} \neq 0, \hbar_{\psi_4} \neq 0$, and $\hbar_{\psi_5} \neq 0$, while the non-zero auxiliary functions are expressed as $H_{\psi_1}, H_{\psi_2}, H_{\psi_3}, H_{\psi_4}$, and H_{ψ_5}, and $\varsigma \in [0,1]$ is the embedding parameter.

From Equations (30)–(34), it is observed that when $\varsigma = 0$ there is

$$\widehat{\psi}_1(\varsigma,0) = \widehat{\psi}_{1,0}(\varsigma), \widehat{\psi}_2(\varsigma,0) = \widehat{\psi}_{2,0}(\varsigma), \widehat{\psi}_3(\varsigma,0) = \widehat{\psi}_{3,0}(\varsigma), \widehat{\psi}_4(\varsigma,0) = \widehat{\psi}_{4,0}(\varsigma), \widehat{\psi}_5(\varsigma,0) = \widehat{\psi}_{5,0}(\varsigma). \tag{45}$$

As $\varsigma = 1$ and $\hbar_{\psi_1} \neq 0, \hbar_{\psi_2} \neq 0, \hbar_{\psi_3} \neq 0, \hbar_{\psi_4} \neq 0$, $\hbar_{\psi_5} \neq 0$ and $H_{\psi_1} \neq 0, H_{\psi_2} \neq 0, H_{\psi_3} \neq 0$, $H_{\psi_4} \neq 0, H_{\psi_5} \neq 0$, then Equations (30)–(34) are obtained as

$$\widehat{\psi}_1(\varsigma,1) = \widehat{\psi}_1(\varsigma), \widehat{\psi}_2(\varsigma,1) = \widehat{\psi}_2(\varsigma), \widehat{\psi}_3(\varsigma,1) = \widehat{\psi}_3(\varsigma), \widehat{\psi}_4(\varsigma,1) = \widehat{\psi}_4(\varsigma), \widehat{\psi}_5(\varsigma,1) = \widehat{\psi}_5(\varsigma),$$

In order to get mth- order deformation equations, Equations (30)–(34) are differentiated m- times with respect to ς, after substituting $\varsigma = 0$ and dividing both sides by $m!$. Finally, the mth- order deformation equations take the following forms:

$$L_{\psi_1}[\psi_{1,m}(\varsigma) - \chi_m\psi_{1,m-1}(\varsigma)] = \hbar_{\psi_1}R_{1,m}(\varsigma). \tag{46}$$

$$L_{\psi_2}[\psi_{2,m}(\varsigma) - \chi_m\psi_{2,m-1}(\varsigma)] = \hbar_{\psi_2}R_{3,m}(\varsigma). \tag{47}$$

$$L_{\psi_3}\Big[\psi_{3,m}(\varsigma) - \chi_{\psi_3}h_{\psi_3-1}(\varsigma)\Big] = \hbar_{\psi_3}R_{3,m}(\varsigma). \tag{48}$$

$$L_{\psi_4}\Big[\psi_{4,m}(\varsigma) - \chi_{\psi_4}h_{\psi_4-1}(\varsigma)\Big] = \hbar_{\psi_4}R_{4,m}(\varsigma). \tag{49}$$

$$L_{\psi_5}\Big[\psi_{5,m}(\varsigma) - \chi_{\psi_5}h_{\psi_5-1}(\varsigma)\Big] = \hbar_{\psi_5}R_{5,m}(\varsigma). \tag{50}$$

with boundary conditions

$$\widehat{\psi}_{1,m}(1) = -\mu_2\widehat{\psi}_{1,m}^{/}(1), \widehat{\psi}_{1,m}(0) - 1 = \mu_1\widehat{\psi}_{1,m}^{/}(0) \tag{51}$$

$$\widehat{\psi}_{2,m}(1) = -\mu_2\widehat{\psi}_{2,m}^{/}(1), \widehat{\psi}_{2,m}(0) - 1 = \mu_1\widehat{\psi}_{2,m}^{/}(0) \tag{52}$$

$$\widehat{\psi}_{3,m}^{/}(0) = \mu_1\widehat{\psi}_{3,m}^{//}(0) =, \widehat{\psi}_{3,m}(0) = 0, \widehat{\psi}_{3,m}(1) = 0, \widehat{\psi}_{3,m}^{/}(1) = -\mu_2\widehat{\psi}_{3,m}^{//}(1) \tag{53}$$

$$\widehat{\psi}_{4,m}^{/}(0) = \mu_1\widehat{\psi}_{4,m}^{//}(0) =, \widehat{\psi}_{4,m}(0) = 0, \widehat{\psi}_{4,m}(1) = 0, \widehat{\psi}_{4,m}^{/}(1) = -\mu_2\widehat{\psi}_{4,m}^{//}(1) \tag{54}$$

$$\widehat{\psi}_{5,m}(1) = -\mu_2\widehat{\psi}_{5,m}^{/}(1), \widehat{\psi}_{5,m}(0) - 1 = \mu_1\widehat{\psi}_{5,m}^{/}(0) \tag{55}$$

where

$$R_{1,m}(\varsigma) = \psi_{1,m-1}^{//} - R\sum_{k=0}^{m-1}\psi_{1,m-1}\psi_{3,k}^{/} + R\sum_{k=0}^{m-1}\psi_{3,m-1}\psi_{1,k}^{/} \tag{56}$$

$$R_{2,m}(\varsigma) = \psi_{2,m-1}^{//} + R\sum_{k=0}^{m-1}\psi_{3,m-1}\psi_{2,k}^{/} \tag{57}$$

$$R_{3,m}(\varsigma) = \psi^{////}_{3,m-1} - R\sum_{k=0}^{m-1} \psi^{/}_{3,m-1}\psi^{//}_{3,k} + R\sum_{k=0}^{m-1} \psi_{3,m-1}\psi^{///}_{3,k} \tag{58}$$

$$R_{4,m}(\varsigma) = \psi^{////}_{4,m-1} - 2R\sum_{k=0}^{m-1} \psi_{4,m-1}\psi^{///}_{4,k} - M^2\sum_{k=0}^{m-1} \psi^{/}_{4,k} \tag{59}$$

$$R_{5,m}(\varsigma) = \psi^{//}_{5,m-1} - R\sum_{k=0}^{m-1} \psi_{5,m-1}\psi^{/}_{4,k} - 2\sum_{k=0}^{m-1} \psi_{4,m-1}\psi^{//}_{5,k} - M^2\psi_5 \tag{60}$$

A well-known software called MATHEMATICA has been used to solve the modeled problem.

4. Convergence Criteria

HAM was applied to compute the solution of the problems given in Equations (7)–(9), (20), and (21), as HAM contains the non-zero auxiliary parameter $\hbar_i (i = 1-5)$, which ensures the convergence of the solution. To get a suitable value for the $\hbar_i$, $\hbar_i-$ curves are displayed. To guarantee the convergence, 20th order $\hbar_i-$ curves have been drawn in Figures 2–6. It can easily be seen from the $\hbar_i$ curves that the acceptable values of $\hbar_i$ were $0.5 \le \hbar_1 \le 1.5$, $-1.5 \le \hbar_2 \le -0.5$, $0 \le \hbar_3 \le 6$, for the long slider. Similarly, acceptable values for the circular slider were $0.5 \le \hbar_4 \le 1.5$, $-1 \le \hbar_5 \le 4$.

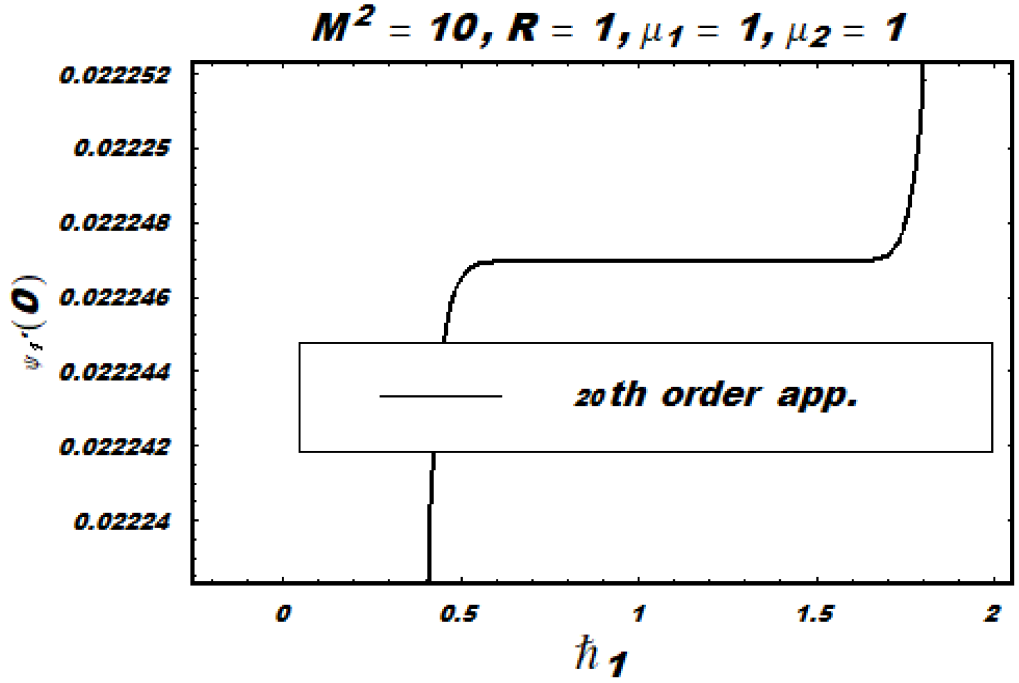

Figure 2. $\hbar_1$ for the strip/long slider.

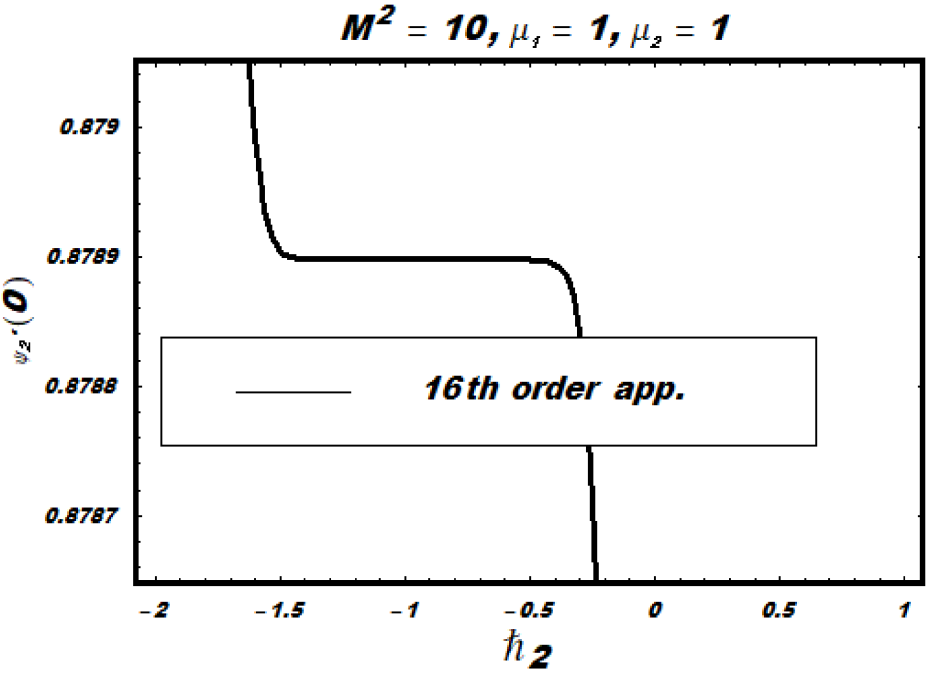

Figure 3. $\hbar_2$ for the strip/long slider.

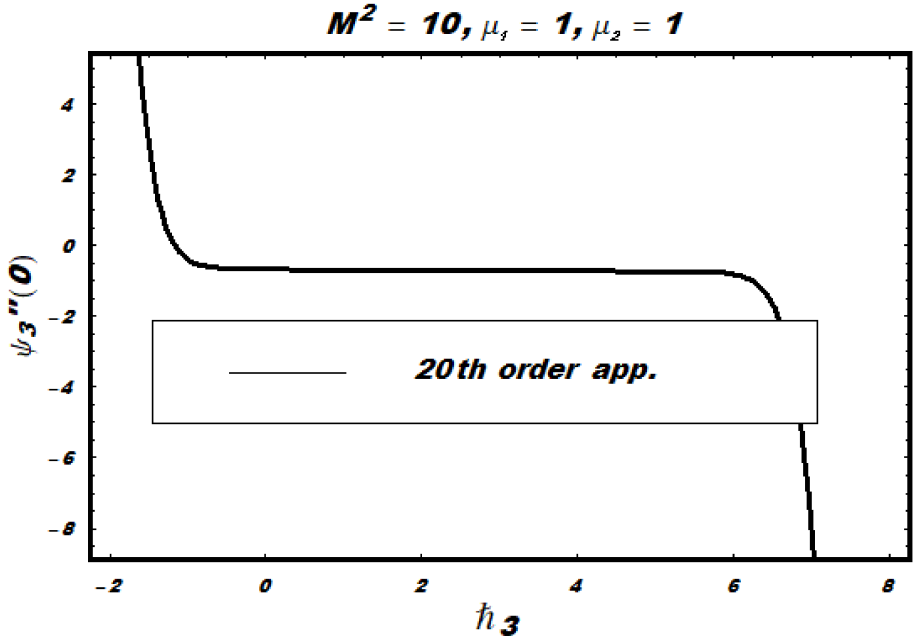

Figure 4. $\hbar_3$ for the strip/long slider.

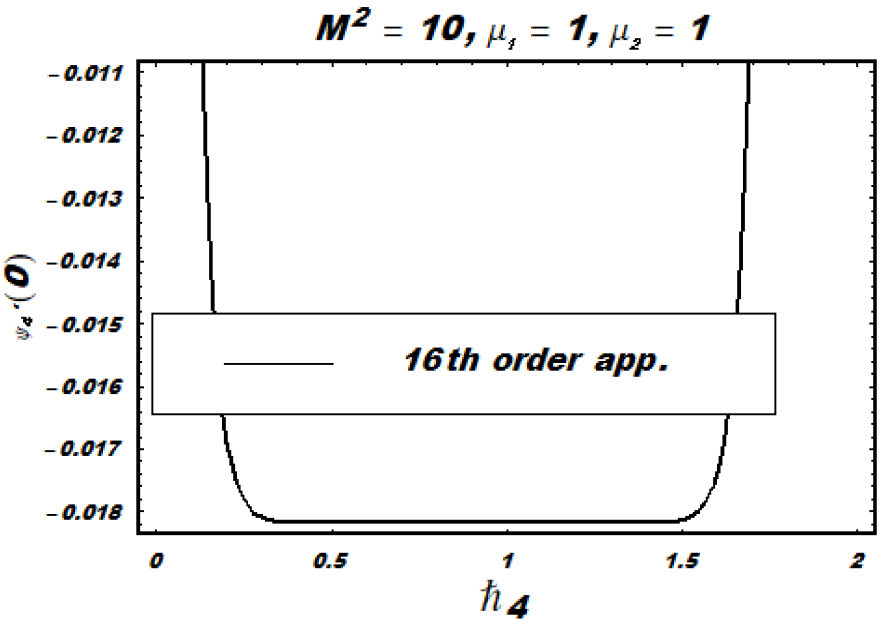

Figure 5. $\hbar_4$ for the circular slider.

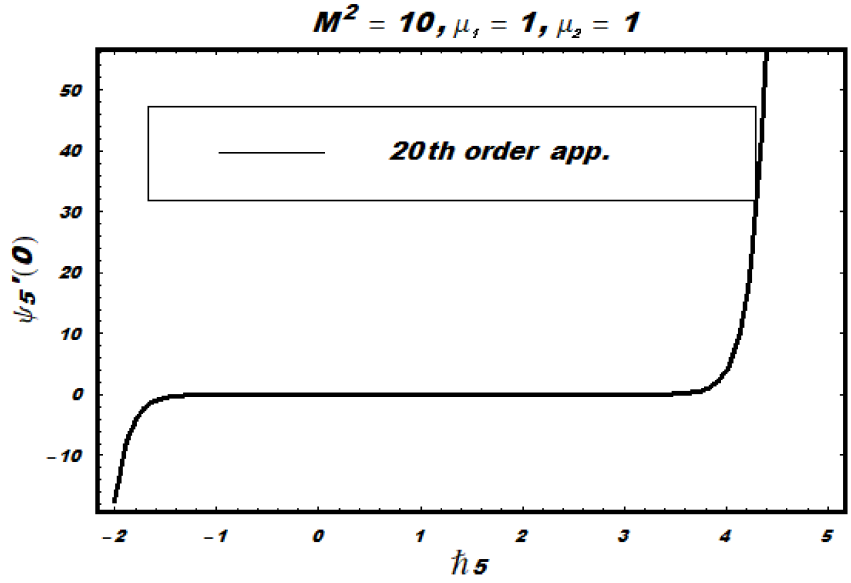

Figure 6. $\hbar_5$ for the circular slider.

5. Results and Discussion

The obtained results from the above-mentioned method (HAM) are presented in the form of tables and graphs. Tables 1 and 2 display the effects of the slip on the dynamic properties of a slider, showing that normalized lift and drag decrease as the slip and/or Reynolds number increases. The lift (per area) of the strip slider was much greater than the circular slider, although the drag remained the same in both cases. The effect of slip could be substantial, affecting the drag much more than the lift.

Table 1. Properties of the long porous slider. Normalized lift Λ, normalized x_1- direction drag, and normalized x_2- direction drag.

β_1,β_2	M^2	R	Λ	$-\psi_1^{/}(1)$	$-\psi_2^{/}(1)$
0, 0	0	0.2	62.33	0.896	0.932
-	-	0.5	26.34	0.760	0.836
-	-	2.0	8.412	0.334	0.467
-	-	5.0	4.917	0.063	0.123
-	-	20	3.267	0	0
-	-	50	2.909	0	0
0.1, 0.1	2	0.2	39.27	0.743	0.780
-	4	0.5	16.78	0.626	0.704
-	6	2.0	6.596	0.4372	0.2536
-	10	5.0	3.436	0.3245	0
	20	20.0	2.440	0.1520	0
	50	50.0	2.240	0	0
0.1, 1	2	0.2	20.31	0.424	0.463
-	4	0.5	8.859	0.357	0.436
-	6	2.0	3.159	0.160	0.321
-	10	5.0	2.050	0.035	0.123
	20	20.0	1.513	0	0.0632
	50	50.0	1.391	0	0.012
0.1, 10	2	0.2	5.316	0.064	0.082
-	4	0.5	2.702	0.046	0.080
-	6	2.0	1.413	0.013	0
-	10	5.0	1.175	0.002	0
	20	20.0	1.068	0	0
	50	50.0	1.047	0	0
1, 1	2	0.2	9.727	0.275	0.315
-	4	0.5	4.591	0.210	0.288
-	6	2.0	2.048	0.068	0.172
	10	5.0	1.569	0.011	0.047
	20	20.0	1.355	0	0
	50	50.0	1.315	0	0

Table 2. Properties of the circular porous slider. Normalized lift Λ, normalized drag $-\psi_1'(1)$.

β_1,β_2	M^2	R	Λ	$-\psi_1'(1)$
0, 0	0	0.2	30.78	0.914
-	-	0.5	12.79	0.797
-	-	2.0	3.833	0.392
-	-	5.0	2.019	0.085
-	-	20	1.349	0
-	-	50	1.194	0
0.1, 0.1	2	0.2	19.33	0.761
-	4	0.5	8.089	0.663
-	6	2.0	2.503	0.310
-	10	5.0	1.445	0.1014
	20	20.0	0.994	0
	50	50.0	0.908	0
0.1, 1	2	0.2	9.853	0.441
-	4	0.5	4.130	0.394
-	6	2.0	1.288	0.129
-	10	5.0	0.752	0.0145
	20	20.0	0.529	0
	50	50.0	0.483	0
0.1, 10	2	0.2	6.438	0.084
-	4	0.5	2.699	0.076
-	6	2.0	0.841	0.015
-	10	5.0	0.488	0
	20	20.0	0.338	0
	50	50.0	0.305	0
1, 1	2	0.2	4.611	0.294
-	4	0.5	2.043	0.244
-	6	2.0	0.776	0.0215
	10	5.0	0.549	0
	20	20.0	0.466	0
	50	50.0	0.453	0

Velocity distributions for the long and circular slider are presented graphically in Figures 7–9.

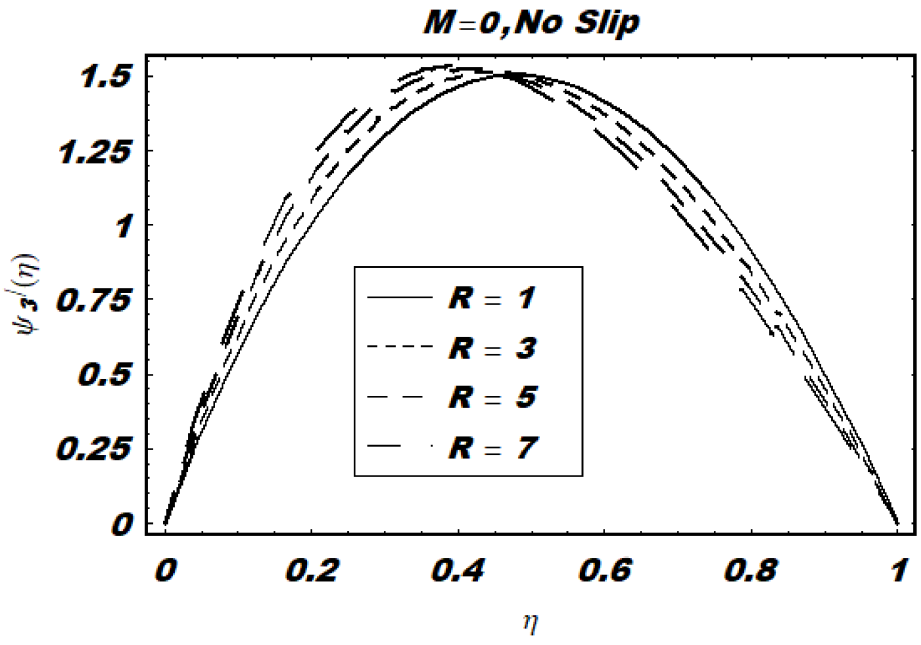

Figure 7. Similarity function ψ_3' for the long slider.

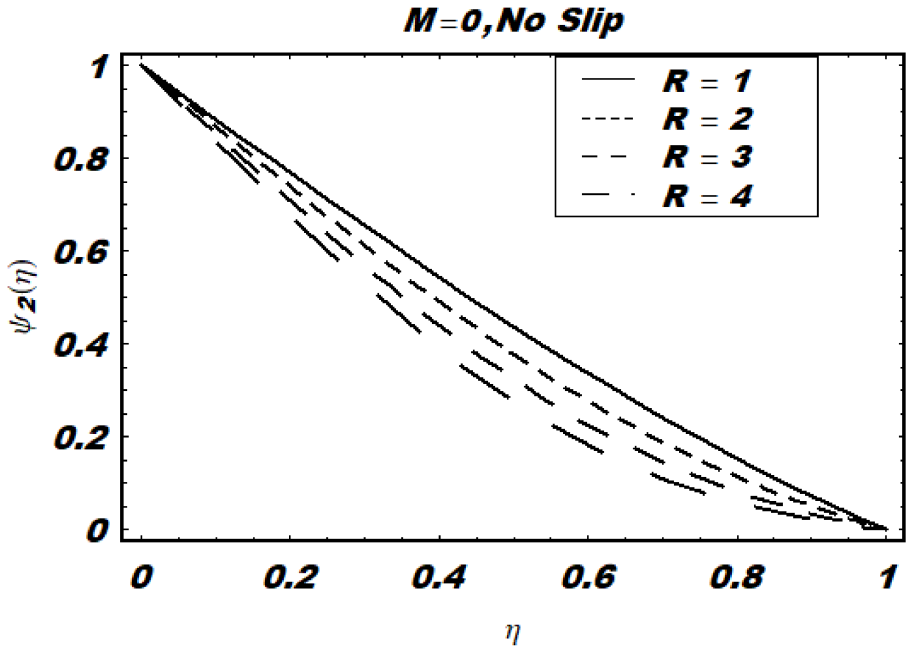

Figure 8. Similarity function ψ_2 for the long slider.

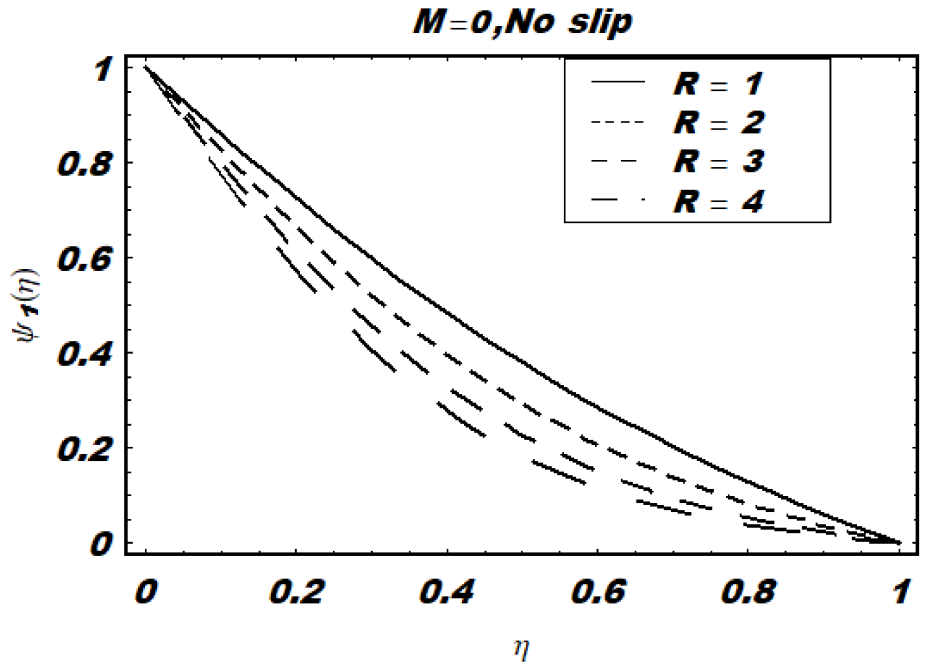

Figure 9. Similarity function ψ_1 for the long slider.

For the long slider, the effect of the Reynolds number in the presence of slip and the magnetic field is shown in Figures 10–18. It is observed that the velocity profile was very much changed. It was seen that slip near the ground reduced the lateral velocity much more than slip on the slider. Moreover, increasing the magnetic parameter decreased the lateral velocity components further (see Figure 12). The effects of the Reynolds number on the typical velocity distribution for the circular slider were similar, as displayed in Figures 19–28. The behavior of velocity profiles was similar for the long and circular sliders in cases of no-slip (see Figures 19 and 20). Further, velocity profiles behaved in a similar fashion in both cases (i.e., parabolic or linear for a low Reynolds number, while a boundary layer formed near the surface in cases of a large Reynolds number). Figures 21–28 demonstrate the effect of

the slip parameter on the velocity components corresponding to different Reynolds numbers. These pictorial descriptions demonstrate that velocity profiles decrease with an increase in slip parameters, and that this decrease become even greater after applying the magnetic field. This is due to the fact that slip hinders fluid particles and displaces motion in the vicinity.

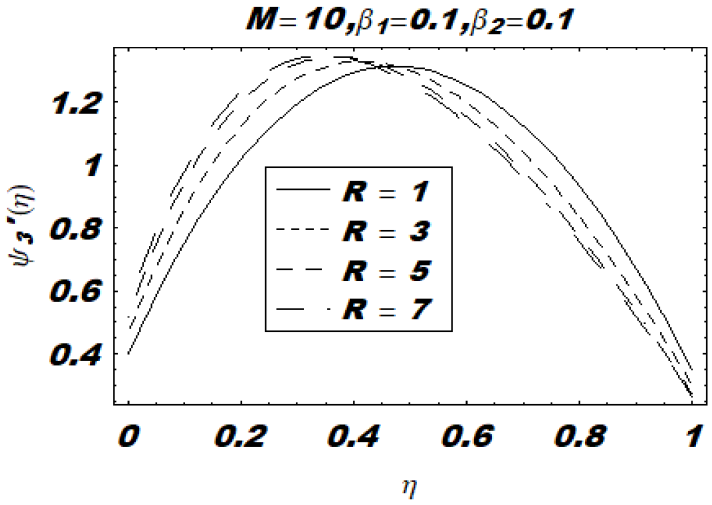

Figure 10. Similarity function $\psi_3^{/}$ for the long slider.

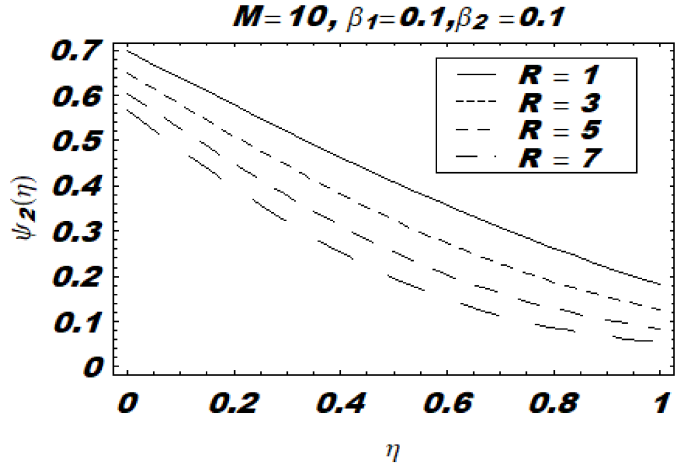

Figure 11. Similarity function ψ_2 for the long slider.

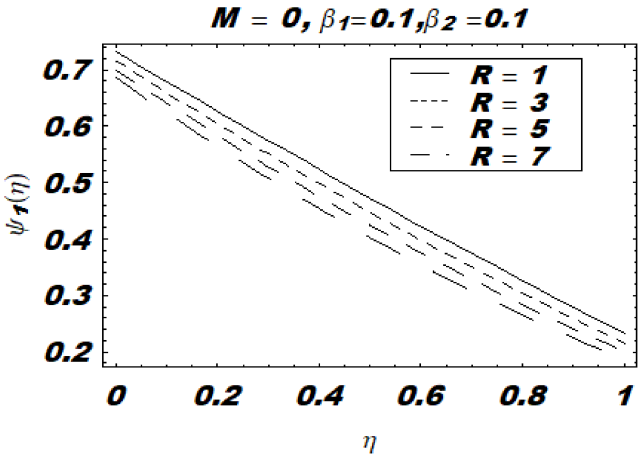

Figure 12. Similarity function ψ_1 for the long slider.

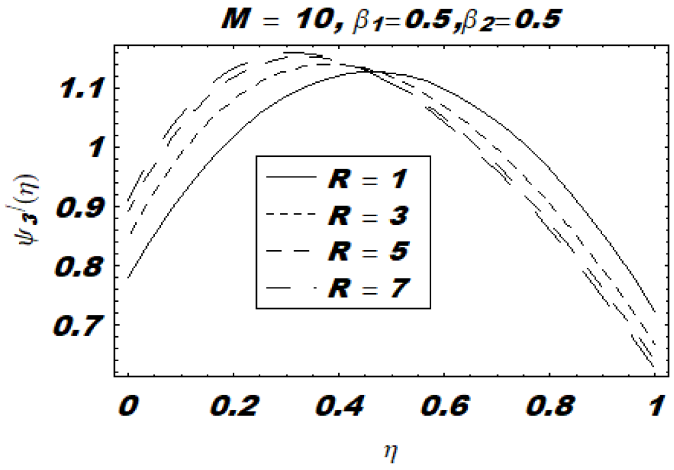

Figure 13. Similarity function $\psi_3^{/}$ for the long slider.

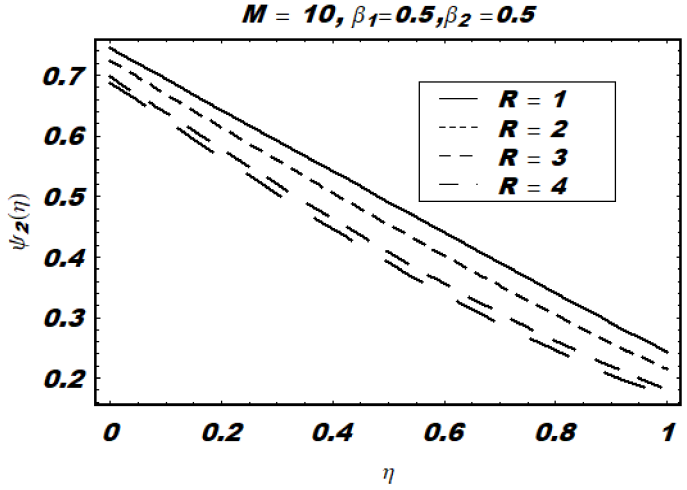

Figure 14. Similarity function ψ_2 for the long slider.

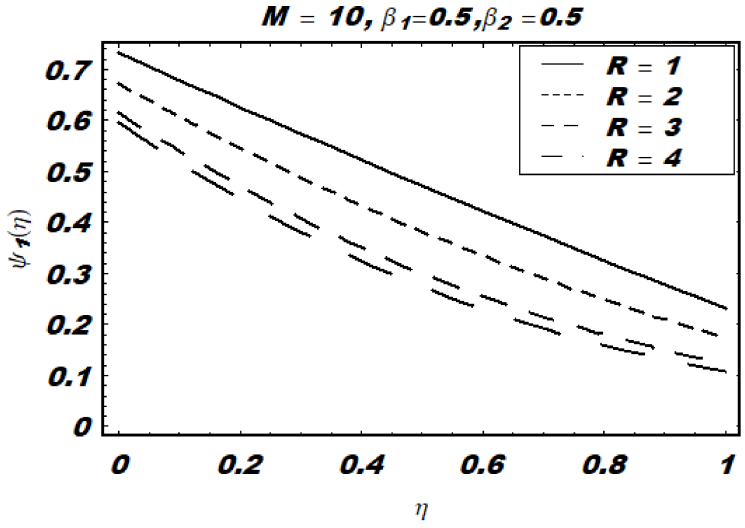

Figure 15. Similarity function ψ_1 for the long slider.

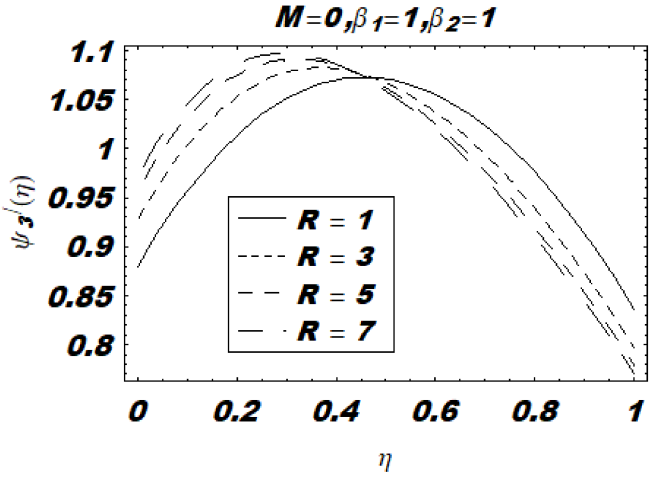

Figure 16. Similarity function $\psi_3^{/}$ for the long slider.

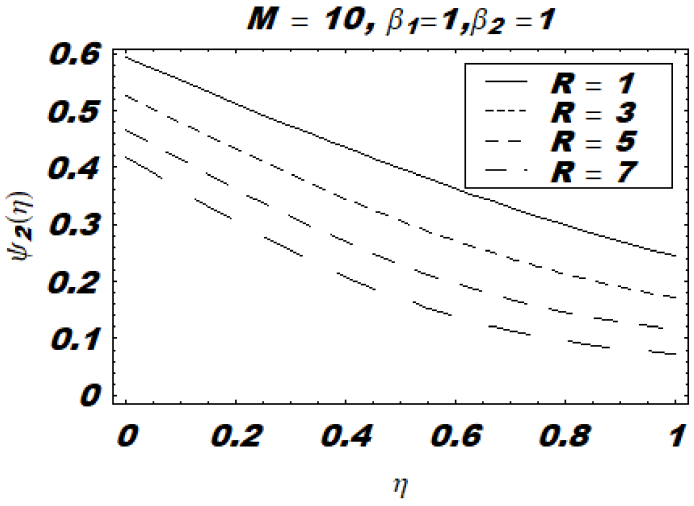

Figure 17. Similarity function ψ_1 for the long slider.

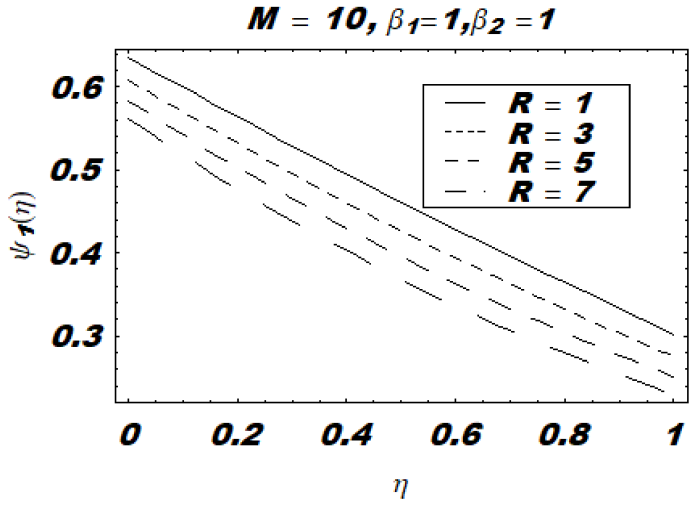

Figure 18. Similarity function $\psi_3^{/}$ for the long slider.

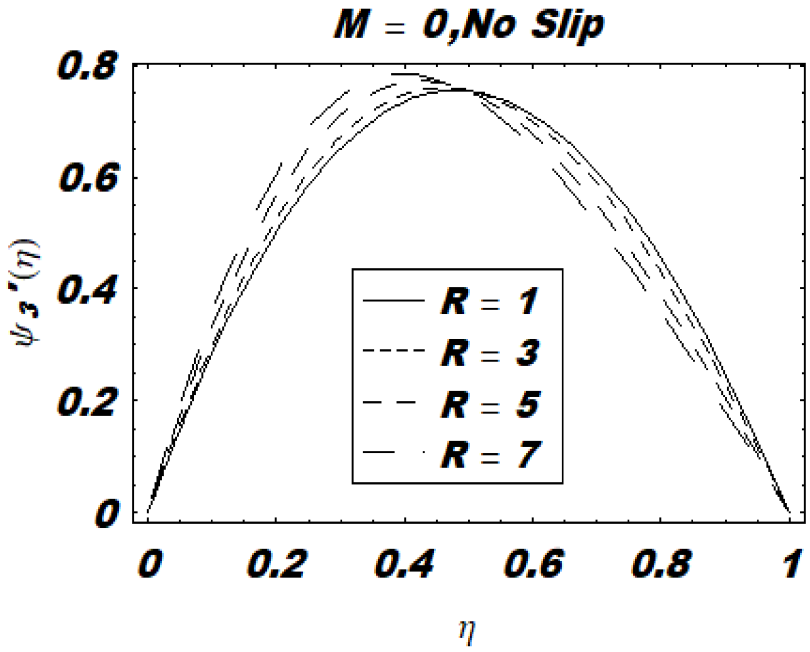

Figure 19. Similarity function $\psi_3^{/}$ for the circular slider.

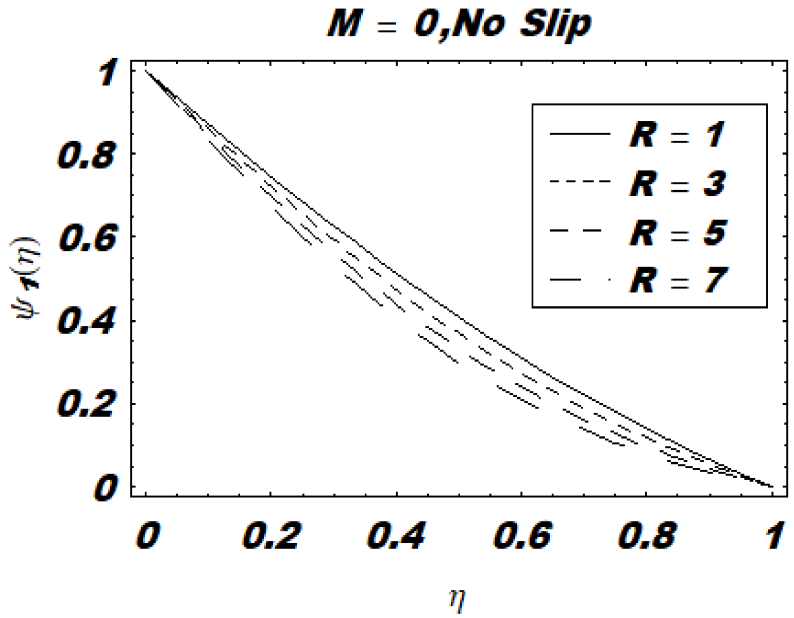

Figure 20. Similarity function ψ_1 for the circular slider.

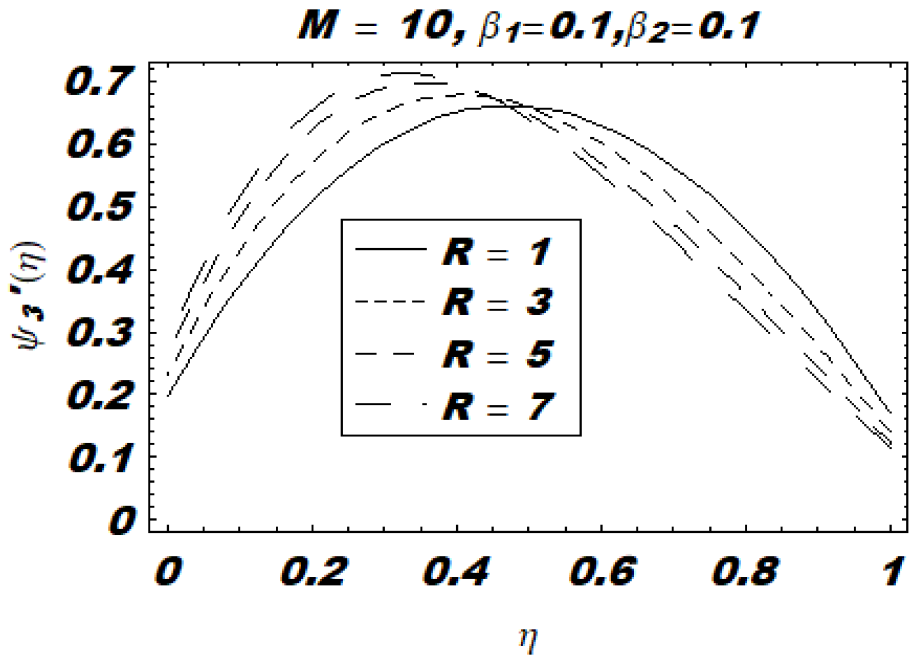

Figure 21. Similarity function $\psi_3^{/}$ for the circular slider.

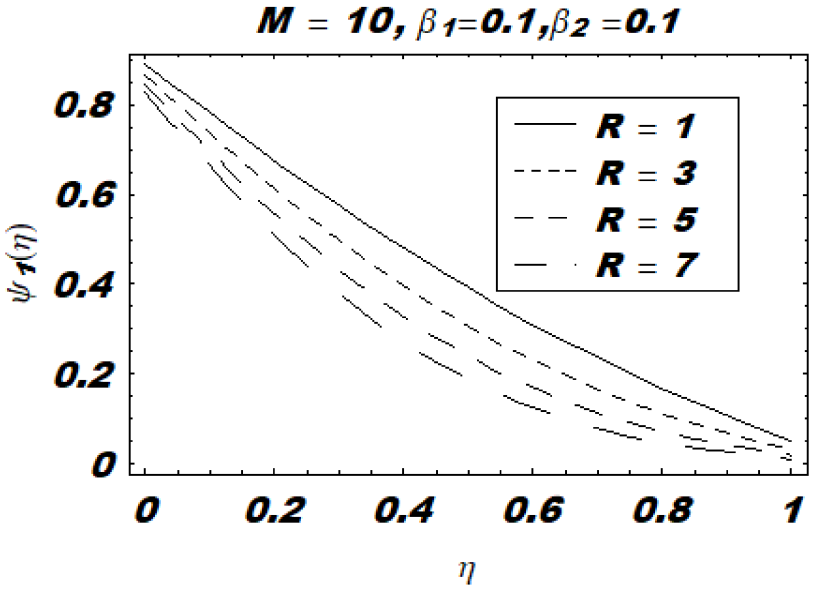

Figure 22. Similarity function ψ_1 for the circular slider.

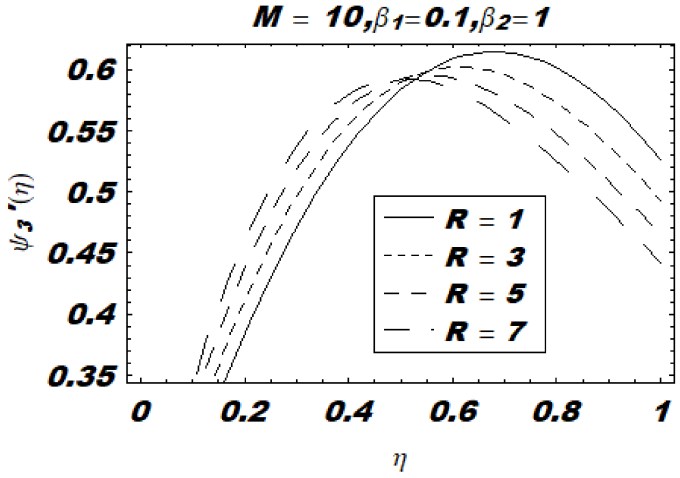

Figure 23. Similarity function $\psi_3^{/}$ for the circular slider.

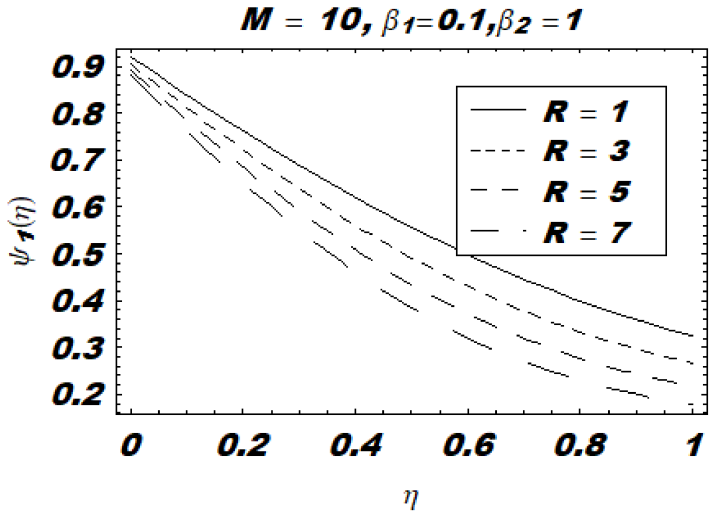

Figure 24. Similarity function ψ_1 for the circular slider.

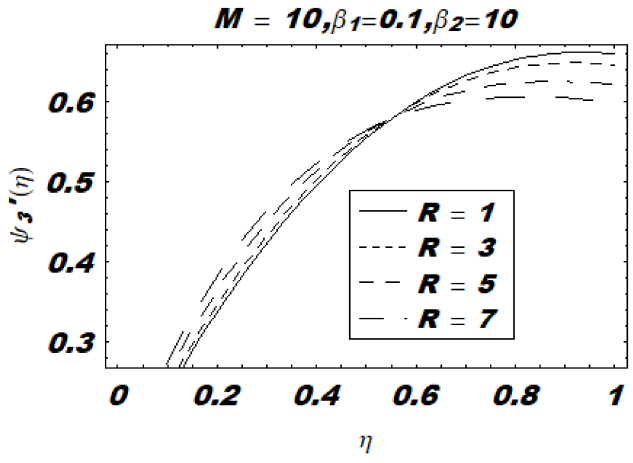

Figure 25. Similarity function $\psi_3^{/}$ for the circular slider.

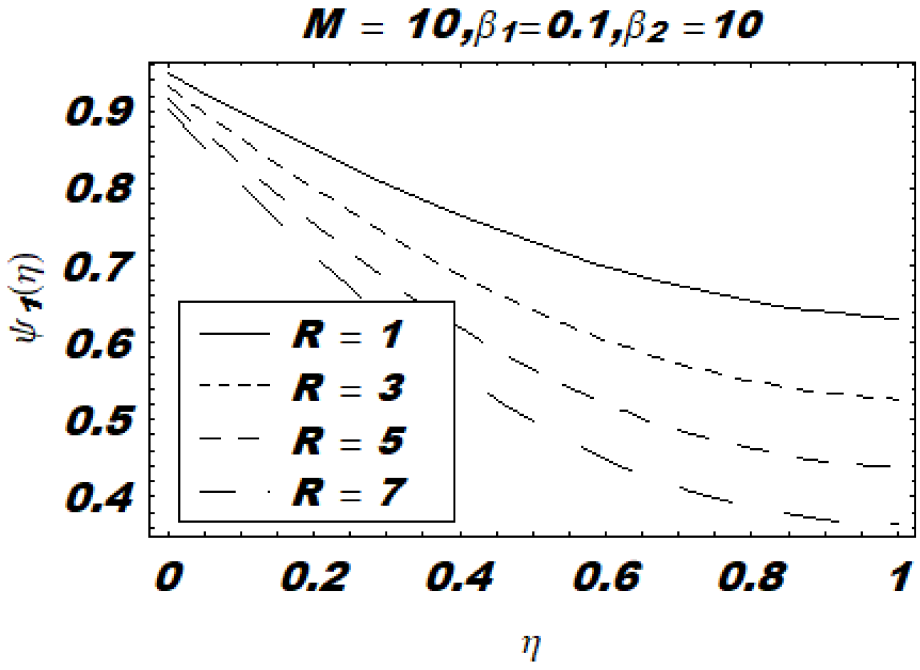

Figure 26. Similarity function ψ_1 for the circular slider.

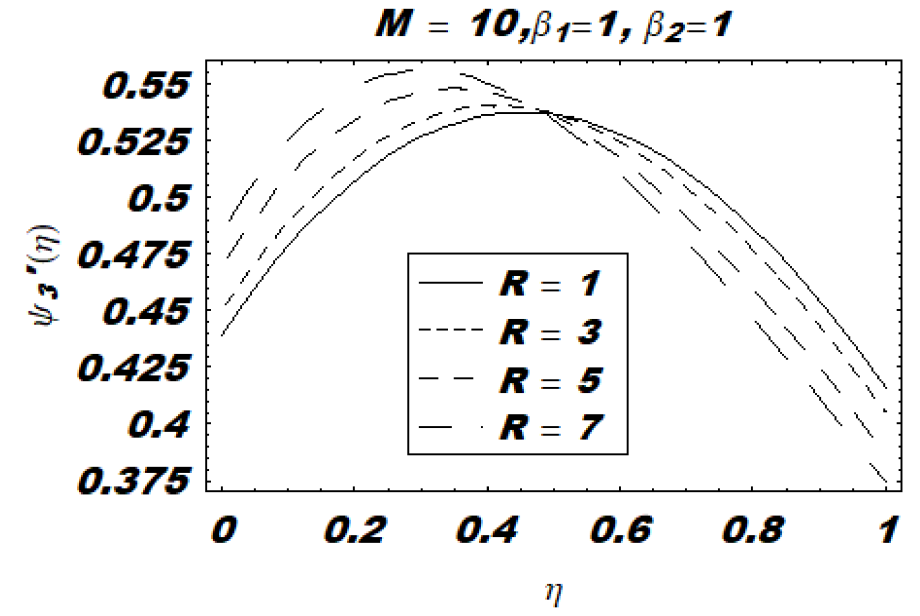

Figure 27. Similarity function $\psi_3^{/}$ for the circular slider.

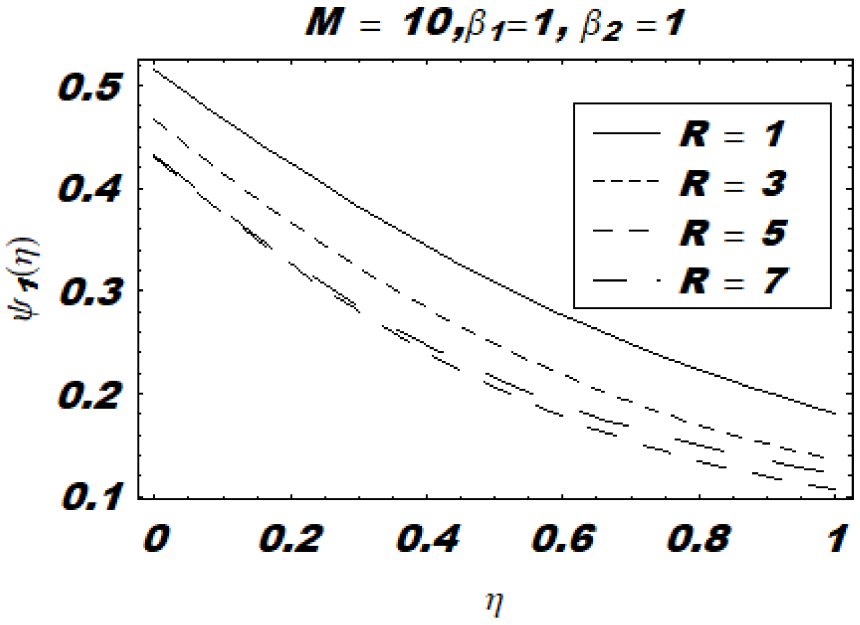

Figure 28. Similarity function ψ_1 for the circular slider.

These results qualitatively confirm the expectation that a drag-like Lorentz force is created by the magnetic field normal to the lateral flow direction, and this force decreases the lateral velocity components. Lift and drag components are important physical quantities for a porous slider. It is interesting to note that the lift is free of translation, but the drag components depend on a cross flow. The effectiveness of a porous slider can be enhanced by making the ratio of friction force to lift smaller. As pointed out by Wang [16], the porous slider should be operated at a cross-flow Reynolds number below unity for optimum efficiency. According to Table 1, porous sliders should be operated at small values that are still valid even when an external uniform magnetic field is applied. Moreover, from the point of view of optimum efficiency, it is more efficient to move a flat slider on a fluid subject than in a high-intensity magnetic field.

6. Conclusions

In this research, different studies have been complied altogether. Different researchers have analyzed fluid flow on a long slider without slip, while others were interested only in a circular slider without slip. Wang presented a comparative study of the both sliders and added velocity slip, but did not cover the effects of a magnetic field. As such, one concern of this study was theoretical investigation of a steady three-dimensional flow of a viscous fluid between a porous slider and the ground in the presence of a transverse uniform magnetic field with velocity slip. The effects of different physical parameter values like Reynolds number and magnetic field on the lateral velocity profiles and lift and drag components were presented in graphs and tables in the presence of velocity slip. It is expected that the results of the present study could be useful for the understanding of various technical problems related to porous sliders where magnetic and velocity slip are the main physical parameters. The main findings are as follows:

- It was shown that normalized lift and drag go down as slip and/or the Reynolds number goes up (see Tables 1 and 2). The lift (per area) of a long slider is much greater than a circular slider. The drag remains the same for both sliders.
- Slip near the ground reduces lateral velocity of the slider much more than slip. By increasing the magnetic parameter, the lateral velocity components decrease further.

- The behavior of velocity profiles is similar for the long and the circular sliders in cases of no-slip (i.e., parabolic or linear for a low Reynolds number).
- In cases of a large Reynolds number, a boundary layer formed near the surface, while velocity profiles decreased with an increase in slip parameters, a decrease which grew more pronounced after applying the magnetic field.

Author Contributions: N.F. and Y.K. conducted whole research such as preparation, creation and/or presentation of the published work by those from the original research group, specifically critical review, commentary or revision – including pre- or post-publication stages. A.A. helped to improve the language of the paper. Drew the schematic diagram of the problem, preparation, creation and/or presentation of the published work, specifically visualization/data presentation. M.K. helped to revise the reviewers' comments.

Funding: This work was supported by the International Cultural Exchange School (ICES), Donghua University, West Yan'an Road 1882, Shanghai 200051, China.

Conflicts of Interest: The authors declare no conflict of interest.

Nomenclature

B_0	Magnetic field	μ	Dynamic viscosity
d	Width	η	Similarity variable
H_1, H_2	Slip coefficient	τ	Extra stress tensor
I	Identity tensor	β_1, β_2	Slip factors
l	Length	ψ_1, ψ_2, ψ_3	Velocity function
p	Pressure	ϕ_1, ϕ_2, ϕ_3	Velocity components
v_0	Constant viscosity	ρ	Fluid density
x_1, x_2, x_3	Space coordinates		

References

1. Skalak, F.; Wang, C.-Y. Fluid Dynamics of a Long Porous Slider. *J. Appl. Mech.* **1975**, *42*, 893–894. [CrossRef]
2. Wang, C.-Y. Erratum: "Fluid Dynamics of the Circular Porous Slider." *J. Appl. Mech.* **1974**, *41*, 343–347. *J. Appl. Mech.* **1978**, *45*, 236. [CrossRef]
3. Wang, C.-Y. The Elliptic Porous Slider at Low Crossflow Reynolds Numbers. *J. Lubr. Technol.* **1978**, *100*, 444. [CrossRef]
4. Bhattacharjee, R.C.; Das, N.C. Porous slider bearing lubricated with couple stress mhd fluids. *Trans. Can. Soc. Mech. Eng.* **1994**, *18*, 317–331. [CrossRef]
5. Patel, J.R.; Deheri, G. A study of thin film lubrication at nanoscale for a ferrofluid based infinitely long rough porous slider bearing. *Facta Univ. Ser. Mech. Eng.* **2016**, *14*, 89–99. [CrossRef]
6. Sinha, P.; Adamu, G. Analysis of Thermal Effects in a Long Porous Rough Slider Bearing. *Proc. Natl. Acad. Sci. India Sectoin A Phys. Sci.* **2017**, *87*, 279–290. [CrossRef]
7. Munshi, M.M.; Patel, A.R.; Deheri, G. Analysis of Rough Porous Inclined Slider Bearing Lubricated with a Ferrofluid Considering Slip Velocity. *Int. J. Res. Advent Technol.* **2019**, *7*, 387–396.
8. Lang, J.; Nathan, R.; Wu, Q. Theoretical and experimental study of transient squeezing flow in a highly porous film. *Tribol. Int.* **2019**, *135*, 259–268. [CrossRef]
9. Madalli, V.S.; Bujurke, N.M.; Mulimani, B.G. Lubrication of a long porous slider. *Tribol. Int.* **1995**, *28*, 225–232. [CrossRef]
10. Awati, V.B.; Jyoti, M. Homotopy analysis method for the solution of lubrication of a long porous slider. *Appl. Math. Nonlinear Sci.* **2016**, *1*, 507–516. [CrossRef]
11. Khan, Y.; Faraz, N.; Yildirim, A.; Wu, Q. A Series Solution of the Long Porous Slider. *Tribol. Trans.* **2011**, *54*, 187–191. [CrossRef]
12. Khan, Y.; Wu, Q.; Faraz, N.; Mohyud-Dind, S.T.; Yıldırım, A. Three-Dimensional Flow Arising in the Long Porous Slider: An Analytic Solution. *Z. Nat. A* **2011**, *66*, 507–511.
13. Faraz, N.; Khan, Y.; Lu, D.C.; Goodarzi, M. Integral transform method to solve the problem of porous slider without velocity slip. *Symmetry* **2019**, *11*, 791. [CrossRef]

14. Ghoreishi, M.; Ismail, A.I.B.M.; Rashid, A. The One Step Optimal Homotopy Analysis Method to Circular Porous Slider. *Math. Probl. Eng.* **2012**, *2012*, 135472. [CrossRef]
15. Shukla, S.D.; Deheri, G.M. Rough porous circular convex pad slider bearing lubricated with a magnetic fluid. In *Lecture Notes in Mechanical Engineering*; Springer: Berlin/Heidelberg, Germany, 2014.
16. Wang, C.Y. A porous slider with velocity slip. *Fluid Dyn. Res.* **2012**, *44*, 065505. [CrossRef]
17. Wang, C.-Y. Fluid Dynamics of the Circular Porous Slider. *J. Appl. Mech.* **1974**, *41*, 343. [CrossRef]
18. Faraz, N. Study of the effects of the Reynolds number on circular porous slider via variational iteration algorithm-II. *Comput. Math. Appl.* **2011**, *61*, 1991–1994. [CrossRef]
19. Madani, M.; Khan, Y.; Mahmodi, G.; Faraz, N.; Yildirim, A.; Nasernejad, B. Application of homotopy perturbation and numerical methods to the circular porous slider. *Int. J. Numer. Methods Heat Fluid Flow* **2012**, *22*, 705–717. [CrossRef]
20. Naeem, F.; Yasir, K. Thin film flow of an unsteady Maxwell fluid over a shrinking/stretching sheet with variable fluid properties. *Int. J. Numer. Methods Heat Fluid Flow* **2018**, *28*, 1596–1612.